



HHS Public Access

Author manuscript

J Phys Chem A. Author manuscript; available in PMC 2023 September 27.

Published in final edited form as:

J Phys Chem A. 2023 September 21; 127(37): 7793–7801. doi:10.1021/acs.jpca.3c02708.

Time-Frequency Analysis of Two-Dimensional Electron Spin Resonance Signals

Gyana Ranjan Sahoo^{†,¶}, Aritro Sinha Roy^{†,‡,¶}, Madhur Srivastava^{†,‡}

[†]Department of Chemistry and Chemical Biology, Cornell University, Ithaca, NY, USA - 14853

[‡]National Biomedical Resources for Advanced ESR Technologies (ACERT), Ithaca, NY, USA - 14853

Abstract

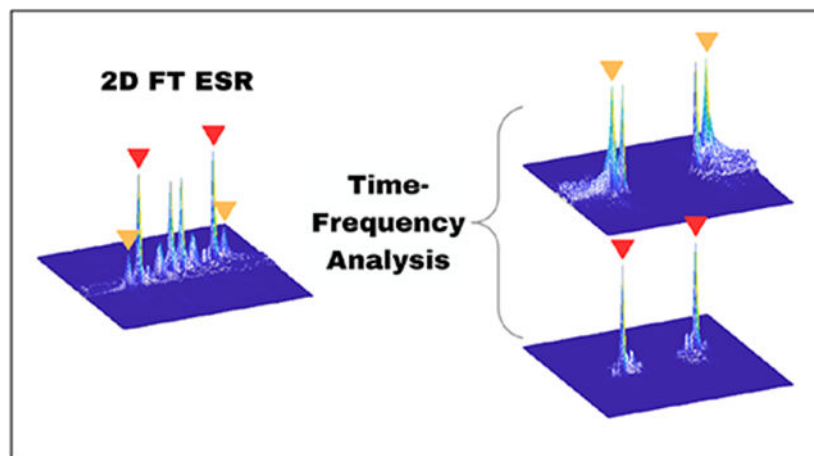
Two dimensional electron spin resonance (2D ESR) spectroscopy is a unique experimental technique in probing protein structure and dynamics, including processes that occur at microsecond time scale. While it provides significant resolution enhancement over the one-dimensional experimental set up, spectral broadening and noise make extraction of spectral information highly challenging. Traditionally, two-dimensional Fourier transform (2D FT) is applied for the analysis of 2D ESR signals, although its efficiency is limited to stationary signals. In addition, it often fails to resolve overlapping peaks in 2D ESR. We propose a time-frequency analysis of 2D time-domain signals in this work, which identifies all the frequency peaks by decoupling a signal into its distinct constituent components via projection on the time-frequency plane. The method utilizes 2D Undecimated Discrete Wavelet Transform (2D UDWT) as an intermediate step in the analysis followed by signal reconstruction and 2D FT. We have applied the method to a simulated 2D double quantum coherence (DQC) signal for validation and a set of experimental 2D ESR signals, demonstrating its efficiency in resolving overlapping peaks in the frequency-domain, while displaying frequency evolution with time in case of non-stationary data.

Graphical Abstract

ms2736@cornell.edu.

[¶]These authors contributed equally

Competing interests: The authors declare that they have no competing interests.



Introduction

Probing protein dynamics is at the heart of understanding their functions in important biological processes.^{1,2} Studying protein dynamics experimentally requires a design that is capable of capturing processes whose rates vary between nano to millisecond time scales. Two dimensional nuclear magnetic resonance (2D NMR) is frequently used in determination of protein structure and dynamics, by probing exchange between different chemical environments. Such experiments are suitable for studying exchange processes which take place over a time scale of millisecond and slower. On the other hand, two dimensional electron spin resonance (2D ESR or 2D ELDOR) is uniquely suited to study much faster real time exchange processes occurring at nanosecond to microsecond time scales.³⁻⁸ Many proteins and biomolecules undergo transitions and conformational changes in this time scale. In both 2D NMR and 2D ESR, exchange phenomena are reflected through the development of crosspeaks in two dimensional frequency-domain spectra. Using nitroxide spin labels, 2D ESR can provide snapshots of both site-specific dynamics and local flexibility of a spin label that is placed at a selected residue on a protein, enabling its dynamics, ordering and relative orientation to be determined in a precise manner.⁹⁻¹³ In principle, 2D ESR can effectively characterize the complex dynamics of proteins occurring at different time scales by using a large range of magnetic fields and frequencies.^{14,15} The most compelling cases are of GPCR and transmembrane proteins, for which experimental data are not available. The reason for that has been the data analysis limitations in studying such systems by 2D ELDOR based on the complexities of the spectra.

Stationary time-domain data is abundant in physical sciences and hence, Fourier transform (FT) has become a natural choice in producing frequency-domain spectra for all types of time-domain signals. However, for non-stationary data, where the frequencies are time-dependent, application of FT results into significant loss of information. In NMR, there are approaches for analyzing non-stationary signals related to studying reaction mechanisms and fast signal acquisitions, among others.¹⁶⁻¹⁹ In this paper, we present a time-frequency analysis of non-stationary 2D signals for separating overlapped peaks. In case of 2D ESR frequency-domain spectra, the data analysis becomes challenging due to the presence of

overlapped and hard-to-distinguish peaks. Two-dimensional Fourier transform (2D FT), which is applied traditionally in the analysis, often fails to achieve desired results due to its inability to achieve the necessary separation between the peaks. Time-frequency analysis²⁰⁻²⁷ is a reliable way for separating the distinct peaks. It decouples a signal into its distinct constituent components by projecting it on the time-frequency plane. The short time Fourier transform (STFT)^{20,21,24} can carry out such analysis, but it is restricted in spectral resolution, similar to FT, due to fixed window length.

Wavelet transforms are powerful methods for time-frequency analysis due to its flexible window length and its applicability to multi-dimensional signals. The advantages of using wavelet-based spectral analysis in both ESR and nuclear magnetic resonance (NMR) spectroscopic studies in one-dimensional experiments have been established,²⁸⁻³⁷ where one can reliably decouple different spectral components, including noise, in separating individual peaks. In this work, we present a 2D undecimated discrete wavelet transform^{38,39} (UDWT)-based approach that can effectively identify and separate overlapping peaks in 2D ESR signals. The current applications of UDWT are primarily based on noise and/or artifact removal, algorithm for which is usually applied either on time or frequency domain.⁴⁰ In our approach, we use 2D UDWT to simultaneously study the time-frequency to decouple overlapped peaks. In this process, a 2D time-domain ESR signal is divided into multiple 2D time-domain signals, each associated with distinct peaks and regions in the spectra. The spectral peaks are then revealed by taking 2D FT of each 2D time-domain signal. It is worth mentioning that the method is general, and can be applied to other 2D signals such as NMR,^{41,42} infrared spectroscopy,^{43,44} FRET^{45,46} among others.^{47,48}

Methods

Description of 2D ESR Data

We used two different types of 2D ESR signals for the time-frequency analysis in this work: (A) simulated 2D double quantum coherence (DQC) data and (B) experimental 2D ELDOR data. The 2D DQC signal is generated for a pair of $S = 1/2$, $I = 1/2$ spin probes, such as ^{15}N -nitroxides, with a 6-pulse sequence and a 256-step phase cycling^{49,50} in solid state. In case of 2D DQC, the two-dimensional Fourier transform (2D FT) of a signal is expected to produce the dipolar interaction between the pair of nitroxides and the nitroxide spectrum along the frequency axes (f_{dip} , f_{echo}).

The DQC data was simulated for a pair of $S = 1/2$, $I = 1/2$ spin probes (^{15}N -nitroxide) in the solid state using the method described here.⁵¹ Figure 1 shows the schematic diagram of a typical 6-pulse sequence and the selected coherence pathway. The time interval, t_{DQ} , is kept fixed (20 ns in this case), while the dipolar signal and the nitroxide echo are recorded over $t_{\text{dip}} = t_m - 2t_p$ and $t_{\text{echo}} = t_3 - t_2$. The dipolar evolution time, $t_m = t_p + t_2$, and the echo window t_w were set to 2 μs and 0.4 μs , respectively. The two parameters t_2 and t_p are varied such that their summation t_m remains constant,⁵⁰ which is the dipolar evolution time. The DQC time-domain signal was calculated by varying t_{dip} between $\pm (t_m - t_w / 2)$ with a time increment of 25 ns and t_{echo} between $\pm t_w$ with a time increment of 1 ns. We used three sets of 2D ELDOR experimental data in this work. The first two experiments used the spin

label, di-tert-butyl nitroxide (DTBN) in a synthetic phospholipid (DMPC) with mixing times of 100 and 400 ns at 40 C. The other 2D ELDOR experimental data is for perdeuterated tempone (PDT) in water recorded at 20 C with a $T_m = 600$ ns. For both the samples, the time-domain signals were recorded by incrementing t_1 from a minimum value of 30 ns to its final value by a step-size of 4 ns over 64 steps, while varying t_2 from 0 to 1.024 μ s with a step-size of 1 ns.

Two Dimensional Undecimated Discrete Wavelet Transform (2D UDWT)

The 2D UDWT is performed on the 2D time-domain ESR signal, which yields N decomposition levels ($N = \min(\text{RowLength}, \text{ColumnLength})$), where each decomposition level contains: 1) Approximation component, 2) Horizontal component, 3) Vertical component, and 4) Diagonal component. This leads to $4 \times N$ wavelet components of 2D time-domain data, each representing distinct time-frequency resolutions. The Approximation components represents the low frequency information of both rows and columns of 2D time-domain data. To start with, the Approximation, Horizontal, Vertical and Diagonal components for an input 2D signal (X) of dimension ($P \times Q$) can be defined as

Approximation component:

$$A_1^c[k, c] = \sum_{c=1}^Q \sum_{n=0}^{L-1} l[n]X[k+n, c] \quad (1)$$

$$A_1[r, k] = \sum_{r=1}^P \sum_{n=0}^{L-1} l[n]A_1^c[r, k+n] \quad (2)$$

Horizontal component:

$$H_1^c[k, c] = \sum_{c=1}^Q \sum_{n=0}^{L-1} l[n]X[k+n, c] \quad (3)$$

$$H_1[r, k] = \sum_{r=1}^P \sum_{n=0}^{L-1} h[n]H_1^c[r, k+n] \quad (4)$$

Vertical component:

$$V_1^c[k, c] = \sum_{c=1}^Q \sum_{n=0}^{L-1} h[n]X[k+n, c] \quad (5)$$

$$V_1[r, k] = \sum_{r=1}^P \sum_{n=0}^{L-1} l[n]V_1^c[r, k+n] \quad (6)$$

Diagonal component:

$$D_i^c[k, c] = \sum_{c=1}^Q \sum_{n=0}^{L-1} h[n]X[k+n, c] \quad (7)$$

$$D_i[r, k] = \sum_{r=1}^P \sum_{n=0}^{L-1} h[n]D_i^c[r, k+n] \quad (8)$$

where A_i^c , H_i^c , V_i^c and D_i^c are the intermediate components, after passing low or high pass filter through each column of the 2D signal, while A_1 , H_1 , V_1 and D_1 represent the Approximation, Horizontal, Vertical and Diagonal components. The parameters $l[n]$ and $h[n]$ are low and high pass signal decomposition filters, respectively. L is the length of both the filters. Figure 2 shows the 2D UDWT process. The low and high pass signal decomposition filters $l[n]$ and $h[n]$ are composed from Coiflet-3 wavelet, because it maximizes the separation between overlapping peaks.

The decomposition level-1 has a broader low time-frequency range, which reduces to narrower range as the decomposition level increases. Hence, it provides time-frequency evolution of the 2D input signal. The Horizontal component represents the low frequency information at each column and high time-frequency information at each row, with frequency band reducing at subsequent decomposition levels. On the other hand, the Vertical component yields the high frequency information for each column and low frequency information for each row. The Diagonal component provides high frequency information for both row and column. The Approximation, Horizontal, Vertical and Diagonal components at the j^{th} -level of decomposition starting with the Approximation component from the $(j-1)^{\text{th}}$ -level are given by

Approximation component:

$$A_j^c[k, c] = \sum_{c=1}^Q \sum_{n=0}^{L-1} l[n]A_{j-1}[k+n, c] \quad (9)$$

$$A_j[r, k] = \sum_{r=1}^P \sum_{n=0}^{L-1} l[n]A_j^c[r, k+n] \quad (10)$$

Horizontal component:

$$H_j^c[k, c] = \sum_{c=1}^Q \sum_{n=0}^{L-1} l[n]A_{j-1}[k+n, c] \quad (11)$$

$$H_j[r, k] = \sum_{r=1}^P \sum_{n=0}^{L-1} h[n] H_j^c[r, k+n] \quad (12)$$

Vertical component:

$$V_j^c[k, c] = \sum_{c=1}^Q \sum_{n=0}^{L-1} h[n] A_{j-1}[k+n, c] \quad (13)$$

$$V_j[r, k] = \sum_{r=1}^P \sum_{n=0}^{L-1} l[n] V_j^c[r, k+n] \quad (14)$$

Diagonal component:

$$D_j^c[k, c] = \sum_{c=1}^Q \sum_{n=0}^{L-1} h[n] A_{j-1}[k+n, c] \quad (15)$$

$$D_j[r, k] = \sum_{r=1}^P \sum_{n=0}^{L-1} h[n] D_j^c[r, k+n] \quad (16)$$

The $4 \times N$ wavelet components yield a comprehensive set of 2D time-domain ESR signals that can be utilized to identify and represent the overlapping peaks.

Peak-Separation via Time-Frequency Analysis

With $4 \times N$ 2D wavelet components representing various time-frequency signals associated with 2D time-domain ESR data, the Fourier spectrum belonging to each of them can be obtained using following steps:

1. Apply undecimated discrete wavelet transform on the 2D time-domain ESR signal, yielding N number of 2D Approximation, Horizontal, Vertical and Diagonal components each, where N is the maximum number of decomposition level.
2. Reconstruct the 2D time-domain signal from each component by inverse discrete wavelet transform, while zeroing the remaining 2D Approximation, Horizontal, Vertical and Diagonal components.
3. Take 2D FT of each of the reconstructed time-domain signals for the time-frequency analysis, yielding $4 \times N$ 2D spectra.

As the spectral location of each peak remains the same, one can observe the evolution and presence of each peak from decomposition level-1 to decomposition level- N , and from low frequency Approximation component to high frequency Diagonal component. Because of

the distinct time-frequency provided, the overlapped peaks in the original spectrum can be distinguished by visually inspecting the $4 \times N$ FT spectra. The process can be streamlined by first observing the 2D FT spectra associated with decomposition level-1 and in the sequence order of Approximation, Horizontal, Vertical and Diagonal. And following the same procedure to the next decomposition level 2D FT spectra. This allows the visual correlation between all the spectra, as well as demonstrates how an initial 2D FT overlapped spectra decomposed into its constituent components. The process is illustrated in Figure 3.

Results and Discussion

Time-Frequency Analysis of 2D DQC Data

We validate the efficacy of the 2D UDWT time-frequency analysis by applying it on the simulated 2D DQC signal with known frequency components. This is an example of stationary data where 2D FT is used for analysis. Hence, in this case, it is possible to obtain the frequency components along each of the frequency axis by averaging the spectra along the complementary axis. Our goal is to resolve the frequency components by a direct analysis of the two-dimensional data using the time-frequency analysis. Figure 4 shows the two-dimensional time-domain signal and the magnitude mode frequency-domain spectrum obtained by the application of 2D FT. Along the dipolar frequency axis, two pairs of peaks are expected, at ± 4.9 MHz (relatively high intensity) and at ± 9.8 MHz (low intensity), respectively. At decomposition levels of 1 and 2 in Figure 4, the Vertical components separate the low intensity peaks from the rest of the spectra and make them clearly visible. A further resolution near the zero-field splitting can be seen at level 3, which might be highly relevant in case of other types of 2D data analysis. The peaks corresponding to the nitroxide spectrum along the echo dimension get resolved in the Vertical component at decomposition level 2 as well. This demonstrates that the time-frequency analysis can effectively detect the frequency components from both stationary and non-stationary two-dimensional time-domain data and providing significant resolution enhancement over the corresponding 2D FT analysis.

Time-Frequency Analysis of 2D ELDOR Data

2D ELDOR captures dynamic changes up to micro-second timescale by varying the mixing time, T_m and analyzing the changes in the frequency-domain. The major barrier of this approach has been poor resolution of closely located peaks in the frequency-domain and the effect of spectral noise at longer timescales, precluding the detection of low intensity peaks or minor but critical changes in the frequency-domain spectra. The 2D ELDOR spectra of DTBN in DMPC with T_m of 100 ns and 400 ns are shown in Figure 5. The evolution of the frequency-domain spectra with increasing T_m can be seen in the 2D FT analysis. However, the highlighted region (red rectangle) in both the cases show overlapping of the central peaks and determination of exact peak positions become highly uncertain. For the signal with T_m of 100 ns in Figure 5 (1), the decomposition of the Approximation component at level-2 (1B) produced two sets of peaks along the Approximation and Vertical components at level 3 (1C, 1D). The separation of peaks in that region can be seen with an increased T_m of 400 ns, Figure 5 (2) in the 2D FT spectrum and in the corresponding time-frequency analysis. It should be noted that at decomposition level-4 in both the cases, the peaks are further

decomposed into two sets of peaks, appearing at the same location in the frequency-domain with slightly altered relative intensities. Time-frequency analysis enables probing of such minute details, inaccessible to the Fourier transform based analysis, which is crucial in studying protein dynamics and utilizing the full potential of 2D ELDOR studies.

The consistency of the time-frequency analysis is illustrated for the 2D ELDOR study of PDT in water, shown in Figure 6. It can be seen that in the Approximation (C, D) and Vertical (G, H) components at decomposition level -3 and 4 start showing spectral resolution in comparison to the 2D FT spectrum. Two distinct sets of cross peaks are revealed along the Vertical components G and H in Figure 6.

Conclusions

We presented a time-frequency analysis of 2D ESR signals for efficient detection of the distinct peaks in 2D ESR signals. The time-frequency analysis revealed peaks in the frequency-domain which were undetectable by the traditional Fourier transform-based analysis. The method achieves significant resolution enhancement in the frequency-domain through decomposition of the time-domain data along the time-frequency plane. We applied the method to simulated 2D DQC and experimental 2D ELDOR signals; the former being used as the test case with known frequencies and the corresponding analysis validated the accuracy of the results obtained by the time-frequency analysis. Similar treatment of the 2D ELDOR data resulted into peak separation and resolution enhancement, both of which are key achievements in utilizing the unique potential of such studies to reveal critical protein dynamics. Further, this work lays the foundation for simulation-independent 2D ESR spectral analysis, which is essential to study complex proteins and their tertiary structure. This study can be extended to the analysis of any 2D time-domain data and use of more advanced techniques, such as the wavelet packet transform for further resolution enhancement.

Acknowledgement

This research was funded by the National Institute of General Medical Sciences/National Institutes of Health under grant R24GM146107 and in part by the Cornell internal funding.

Data availability:

Data, MATLAB and Python codes used in this work have been stored in the public github repository (<https://github.com/Signal-Science-Lab/Time-Frequency-Analysis-of-2DESR-Signals>).

References

- (1). Boehr DD; Nussinov R; Wright PE The role of dynamic conformational ensembles in biomolecular recognition. *Nature Chemical Biology* 2009, 5, 789–796. [PubMed: 19841628]
- (2). Etzkorn M; Raschle T; Hagn F; Gelev V; Rice AJ; Walz T; Wagner G Cell-free expressed bacteriorhodopsin in different soluble membrane mimetics: biophysical properties and NMR accessibility. *Structure* 2013, 21, 394–401. [PubMed: 23415558]

- (3). Costa-Filho AJ; Shimoyama Y; Freed JH A 2D-ELDOR study of the liquid ordered phase in multilamellar vesicle membranes. *Biophysical Journal* 2003, 84, 2619–2633. [PubMed: 12668470]
- (4). Chiang Y-W; Costa-Filho AJ; Freed JH Dynamic molecular structure and phase diagram of DPPC–cholesterol binary mixtures: A 2D-ELDOR study. *The Journal of Physical Chemistry B* 2007, 111, 11260–11270. [PubMed: 17760438]
- (5). Chiang YW; Costa-Filho A. J. d.; Freed JH Two-dimensional ELDOR in the study of model and biological membranes. *Applied Magnetic Resonance* 2007, 31, 375–386.
- (6). Franck JM; Chandrasekaran S; Dzikovski B; Dunnam CR; Freed JH Focus: Two-dimensional electron-electron double resonance and molecular motions: The challenge of higher frequencies. *The Journal of Chemical Physics* 2015, 142, 212302.
- (7). Earle KA; Dzikovski B; Hofbauer W; Moscicki JK; Freed JH High-frequency ESR at ACERT. *Magnetic Resonance in Chemistry* 2005, 43, S256–S266. [PubMed: 16235203]
- (8). Hofbauer W; Earle K; Dunnam C; Moscicki J; Freed J High-power 95 GHz pulsed electron spin resonance spectrometer. *Review of Scientific Instruments* 2004, 75, 1194–1208.
- (9). Dzikovski B; Tipikin D; Freed J Conformational distributions and hydrogen bonding in gel and frozen lipid bilayers: A high frequency spin-label ESR study. *The Journal of Physical Chemistry B* 2012, 116, 6694–6706. [PubMed: 22324811]
- (10). Lis L; McAlister D; Fuller N; Rand R; Parsegian V Interactions between neutral phospholipid bilayer membranes. *Biophysical Journal* 1982, 37, 657–665. [PubMed: 7074191]
- (11). Smirnov AI; Smirnova TI; Morse P 2nd Very high frequency electron paramagnetic resonance of 2, 2, 6, 6-tetramethyl-1-piperidinyloxy in 1, 2-dipalmitoyl-sn-glycero-3-phosphatidylcholine liposomes: Partitioning and molecular dynamics. *Biophysical Journal* 1995, 68, 2350–2360. [PubMed: 7647239]
- (12). Dzikovski B; Livshits V; Freed J Interaction of spin-labeled lipid membranes with transition metal ions. *The Journal of Physical Chemistry B* 2015, 119, 13330–13346. [PubMed: 26490692]
- (13). Nakagawa K. Electron spin resonance investigation of small spin probes in aqueous and vesicle phases of mixed membranes made from poly (oxyethylene) hydrogenated castor oil and hexadecane. *Lipids* 2005, 40, 745. [PubMed: 16196426]
- (14). Dzikovski B; Khramtsov VV; Chandrasekaran S; Dunnam C; Shah M; Freed JH Microsecond exchange processes studied by two-dimensional ESR at 95 GHz. *Journal of the American Chemical Society* 2020, 142, 21368–21381.
- (15). Gupta P; Liang Z; Freed JH Microsecond dynamics in proteins by two-dimensional ESR: Predictions. *The Journal of Chemical Physics* 2020, 152, 214112. [PubMed: 32505151]
- (16). Nawrocka EK; Kasprzak P; Zawada K; Sadlo J; Grochala W; Kazimierczuk K; Leszczy ski PJ Nonstationary two-dimensional nuclear magnetic resonance: A method for studying reaction mechanisms in situ. *Analytical Chemistry* 2019, 91, 11306–11315. [PubMed: 31387347]
- (17). Romero JA; Nawrocka EK; Shchukina A; Blanco FJ; Diercks T; Kazimierczuk K Non-stationary complementary non-uniform sampling (NOSCO NUS) for fast acquisition of serial 2D NMR titration data. *Angewandte Chemie* 2020, 132, 23702–23705.
- (18). Shchukina A; Malecki P; Mateos B; Nowakowski M; Urbanczyk M; Kontaxis G; Kasprzak P; Conrad-Billroth C; Konrat R; Kazimierczuk K Temperature as an extra dimension in multidimensional protein NMR spectroscopy. *Chemistry–A European Journal* 2021, 27, 1753–1767. [PubMed: 32985764]
- (19). Rytel M; Kasprzak P; Setny P; Kazimierczuk K Quick temperature-sweep pure-shift NMR: The case of solvent effects in atorvastatin. *Physical Chemistry Chemical Physics* 2019, 21, 19209–19215. [PubMed: 31441478]
- (20). Langmead CJ; Donald BR Extracting structural information using time-frequency analysis of protein NMR data. *Proceedings of the fifth Annual International Conference on Computational Biology*. 2001; pp 164–175.
- (21). Daubechies I. The wavelet transform, time-frequency localization and signal analysis. *IEEE Transactions on Information Theory* 1990, 36, 961–1005.
- (22). Popi ski W. Wavelet transform for time-frequency representation and filtration of discrete signals. *Applicationes Mathematicae* 1996, 23, 433–448.

- (23). Constable R; Thornhill R Using the discrete wavelet transform for time–frequency analysis of the surface EMG signal. *Biomedical Sciences Instrumentation* 1993, 29, 121–127. [PubMed: 8329582]
- (24). Brotherton T; Pollard T; Barton R; Krieger A; Marple L Application of time–frequency and time–scale analysis to underwater acoustic transients. [1992] *Proceedings of the IEEE-SP International Symposium on Time-Frequency and Time-Scale Analysis*. 1992; pp 513–516.
- (25). Serrai H; Senhadji L; de Certaines JD; Coatrieux JL Time-domain quantification of amplitude, chemical shift, apparent relaxation time T^*2 , and phase by wavelet-transform analysis. application to biomedical magnetic resonance spectroscopy. *Journal of Magnetic Resonance* 1997, 124, 20–34. [PubMed: 9424306]
- (26). Qin L; He B A wavelet-based time–frequency analysis approach for classification of motor imagery for brain–computer interface applications. *Journal of Neural Engineering* 2005, 2, 65. [PubMed: 16317229]
- (27). Lang WC; Forinash K Time–frequency analysis with the continuous wavelet transform. *American Journal of Physics* 1998, 66, 794–797.
- (28). Ahmed OA; Fahmy MM NMR signal enhancement via a new time–frequency transform. *IEEE Transactions on Medical Imaging* 2001, 20, 1018–1025. [PubMed: 11686437]
- (29). Antoine J-P; Chauvin C; Coron A Wavelets and related time–frequency techniques in magnetic resonance spectroscopy. *NMR in Biomedicine* 2001, 14, 265–270. [PubMed: 11410944]
- (30). Barache D; Antoine J-P; Dereppe J-M The continuous wavelet transform, an analysis tool for NMR spectroscopy. *Journal of Magnetic Resonance* 1997, 128, 1–11.
- (31). Srivastava M. Improving signal resolution and reducing experiment time in electron spin resonance spectroscopy via data processing methods. Ph.D. Thesis, Cornell University, Ithaca, NY, USA, 2018.
- (32). Srivastava M; Dzikovski B; Freed JH Extraction of weak spectroscopic signals with high fidelity: Examples from ESR. *The Journal of Physical Chemistry A* 2021, 125, 4480–4487. [PubMed: 34009996]
- (33). Bekerman W; Srivastava M Enabling dynamics studies of proteins at low concentrations using electron spin resonance. *Biophysical Journal* 2022, 121, 407a.
- (34). Roy AS; Srivastava M Hyperfine decoupling of ESR spectra using wavelet transform. *Magnetochemistry* 2022, 8, 32. [PubMed: 37475982]
- (35). Sinha Roy A; Srivastava M Analysis of small-molecule mixtures by super-resolved ^1H NMR spectroscopy. *The Journal of Physical Chemistry A* 2022, 126, 9108–9113. [PubMed: 36413171]
- (36). Sinha Roy A; Srivastava M Unsupervised analysis of small molecule mixtures by wavelet-based super-resolved NMR. *Molecules* 2023, 28, 792. [PubMed: 36677850]
- (37). Roy AS; Dzikovski B; Dolui D; Makhlynets O; Dutta A; Srivastava M. HA Simulation Independent Analysis of Single- and Multi-Component cw ESR Spectra. *Magnetochemistry* 2023, 9, 112. [PubMed: 37476293]
- (38). Gyaourova A; Kamath C; Fodor IK Undecimated wavelet transforms for image de-noising. Report, Lawrence Livermore National Lab., CA 2002, 18.
- (39). Starck J-L; Fadili J; Murtagh F The undecimated wavelet decomposition and its reconstruction. *IEEE Transactions on Image Processing* 2007, 16, 297–309. [PubMed: 17269625]
- (40). Chambolle A; De Vore RA; Lee N-Y; Lucier BJ Nonlinear wavelet image processing: variational problems, compression, and noise removal through wavelet shrinkage. *IEEE Transactions on Image Processing* 1998, 7, 319–335. [PubMed: 18276252]
- (41). Jain SK; Tabassum T; Li L; Ren L; Fan W; Tsapatsis M; Caratzoulas S; Han S; Scott SL P-site structural diversity and evolution in a zeosil catalyst. *Journal of the American Chemical Society* 2021, 143, 1968–1983. [PubMed: 33491456]
- (42). Jain SK; Rawlings D; Antoine S; Segalman RA; Han S Confinement promotes hydrogen bond network formation and grotthuss proton hopping in ion-conducting block copolymers. *Macromolecules* 2022, 55, 615–622.
- (43). Stingel AM; Petersen PB Couplings across the vibrational spectrum caused by strong hydrogen bonds: A continuum 2D IR study of the 7-azaindole–acetic acid heterodimer. *The Journal of Physical Chemistry B* 2016, 120, 10768–10779. [PubMed: 27669743]

- (44). Stingel AM; Petersen PB Full spectrum 2D IR spectroscopy reveals below-gap absorption and phonon dynamics in the mid-IR bandgap semiconductor InAs. *The Journal of Chemical Physics* 2021, 155, 104202. [PubMed: 34525815]
- (45). Taylor JN; Landes CF Improved resolution of complex single-molecule FRET systems via wavelet shrinkage. *The Journal of Physical Chemistry B* 2011, 115, 1105–1114. [PubMed: 21214275]
- (46). Taylor JN; Makarov DE; Landes CF Denoising single-molecule FRET trajectories with wavelets and Bayesian inference. *Biophysical Journal* 2010, 98, 164–173. [PubMed: 20074517]
- (47). Frostig H; Bayer T; Dudovich N; Eldar YC; Silberberg Y Single-beam spectrally controlled two-dimensional Raman spectroscopy. *Nature Photonics* 2015, 9, 339–343.
- (48). Tokmakoff A; Lang MJ; Larsen D; Fleming GR; Chernyak V; Mukamel S Two-dimensional Raman spectroscopy of vibrational interactions in liquids. *Physical Review Letters* 1997, 79, 2702.
- (49). Borbat PP; Freed JH Double-quantum ESR and distance measurements. *Distance Measurements in Biological Systems by EPR* 2000, 383–459.
- (50). Misra SK; Borbat PP; Freed JH Calculation of double-quantum-coherence two-dimensional spectra: Distance measurements and orientational correlations. *Applied Magnetic Resonance* 2009, 36, 237–258. [PubMed: 20161423]
- (51). Roy AS Pulsed double-quantum coherence electron paramagnetic resonance in protein structure determination. Ph.D. Thesis, Cornell University, Ithaca, NY, USA, 2021.

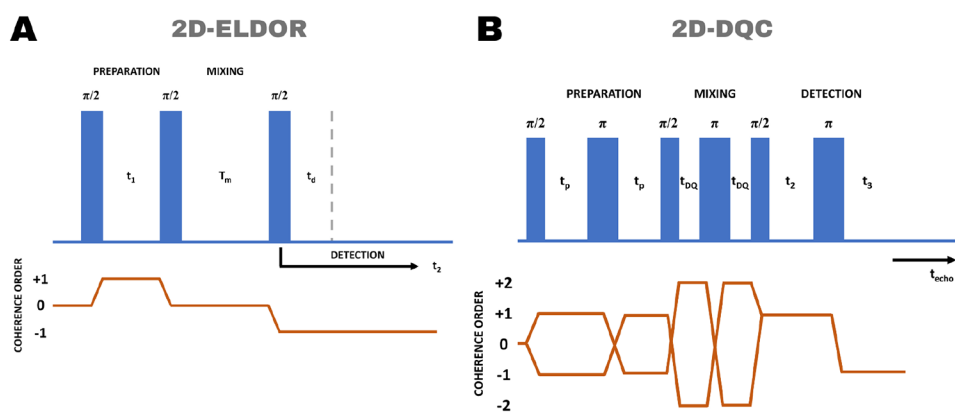


Figure 1: Schematic presentation of (A) 2D ELDOR and (B) 2D DQC pulse sequences and the corresponding coherence pathways. In case of 2D ELDOR, t_d corresponds to the dead-time and the mixing time (T_m) is kept constant in an experiment, while in 2D DQC experiments, t_{DQ} is kept constant.

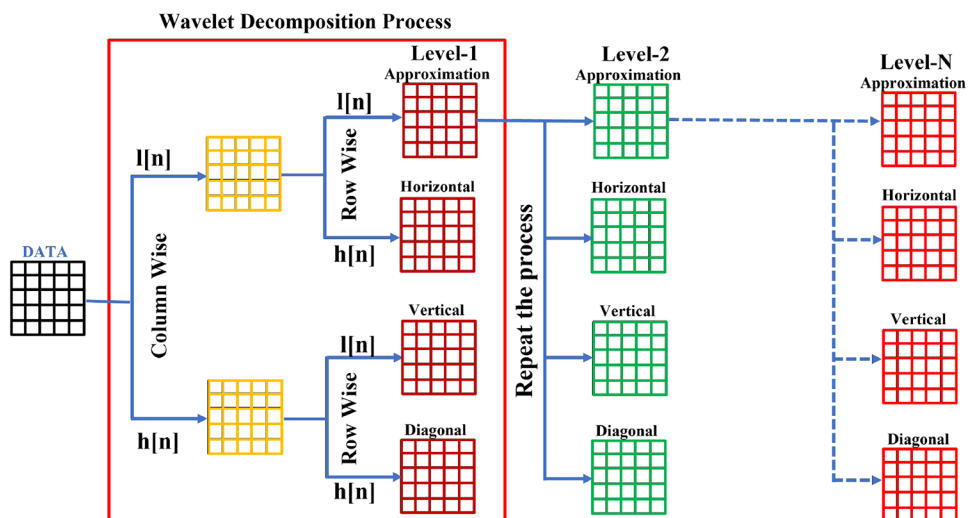


Figure 2: Two dimensional undecimated wavelet decomposition for the time-frequency analysis of a 2D input signal using predefined low-pass ($l[n]$) and high-pass ($h[n]$) filters. Each column of the input data is first passed through $l[n]$ and $h[n]$, yielding two output matrices, followed by repeating the process for each row of the two output matrices, producing the Approximation, Horizontal, Vertical and Diagonal components. For subsequent levels of wavelet decomposition, the process is repeated on the Approximation coefficients.

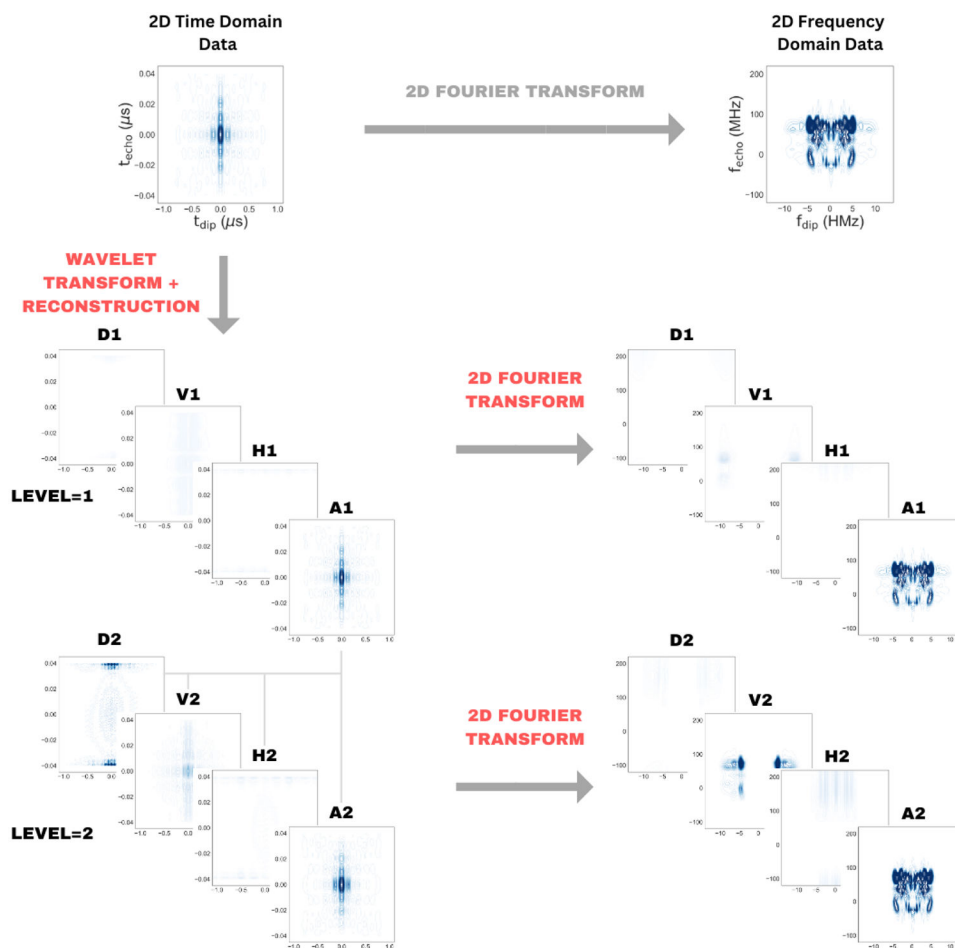


Figure 3: Resolution enhancement of 2D ESR signal by time-frequency analysis. Traditional 2D FT of the signal produces the frequency-domain spectra (top right). In the time-frequency analysis, the time-domain data is decomposed by the wavelet transform using Coiflet-3 wavelet, followed by reconstruction and application of the 2D FT. The spectral decomposition at level-1 and -2 are shown for illustration. Beyond level -1, only the Approximation component from a level is decomposed further and at each level, majority of the spectral information gets distributed between the Approximation and the Vertical components.

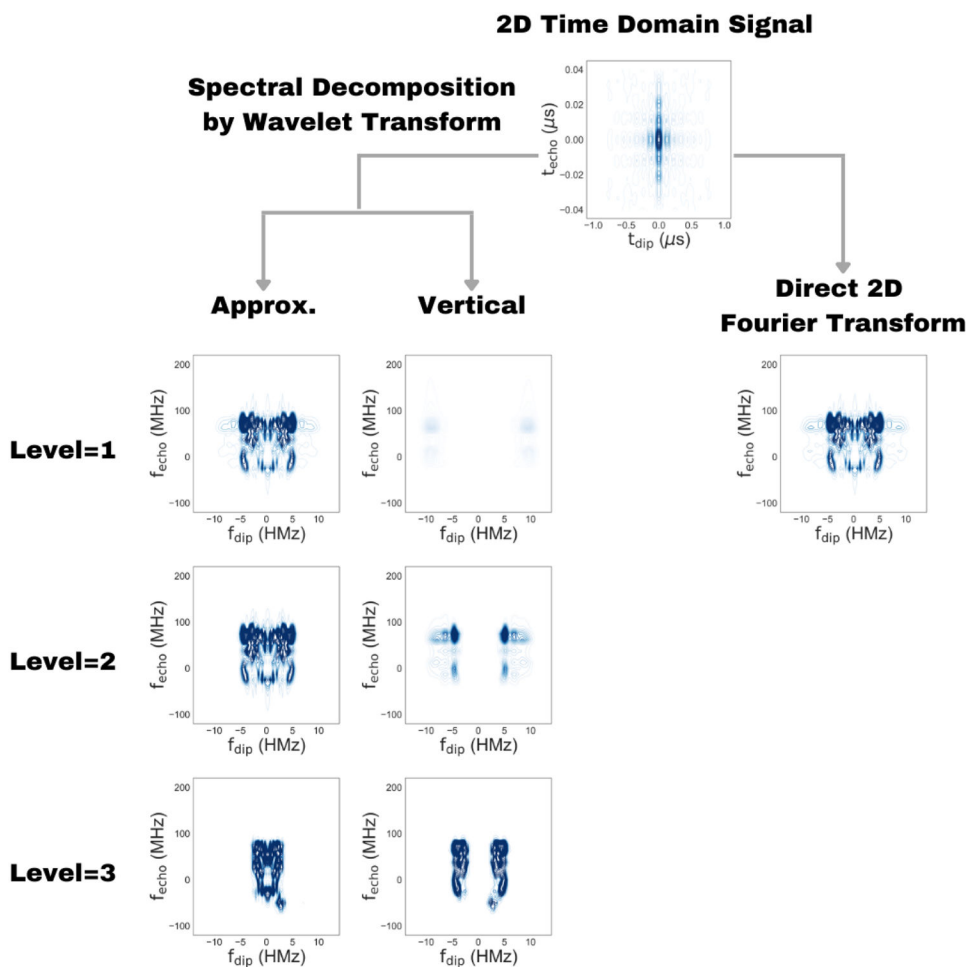


Figure 4: Time-frequency analysis of 2D DQC data using Coiflet-3 wavelet. The magnitude mode 2D FT spectrum is shown on the right and the 2D FT of the reconstructions from the Approximation and Vertical components at different decomposition levels are shown on the left. Decoupling of peaks along both the dipolar and echo dimensions are evident at decomposition level 2 and 3.

2D FT Spectra | Time-Frequency Analysis

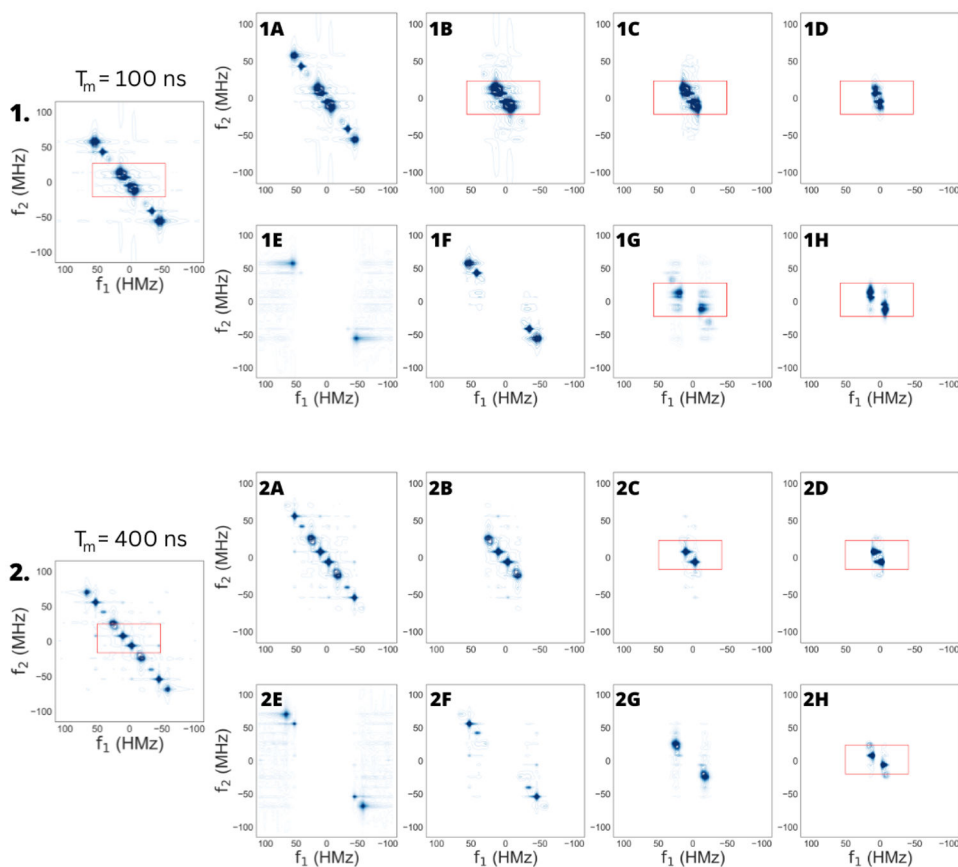


Figure 5: Time-frequency analysis of the real 2D ELDOR signals of DTBN in DMPC at 40 C with mixing time, $T_m =$ (1) 100 ns and (2) 400 ns, respectively. Spectral reconstruction at decomposition levels of 1 to 4 are shown for the Approximation (A–D) and the Vertical (E–H) components. Spectral resolution is achieved in the region of (1) ± 25 MHz and (2) ± 20 MHz (red rectangle) along both the frequency axes at level 3 and 4.

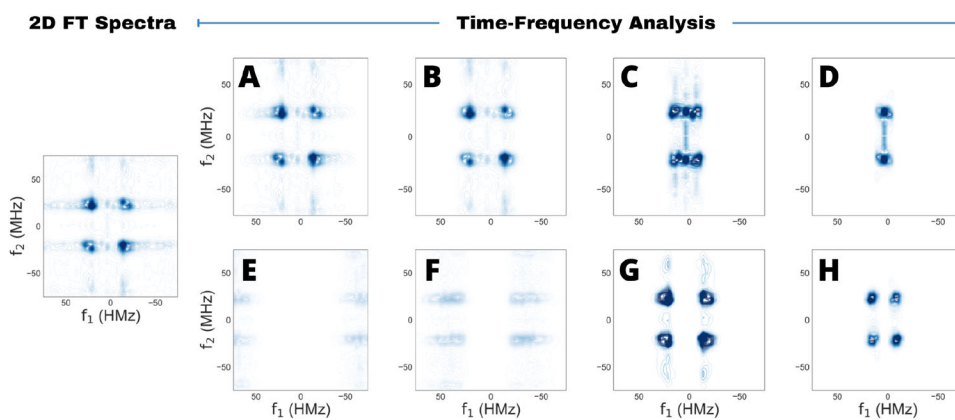


Figure 6: Time-frequency analysis of the real 2D ELDOR signal of PDT in water at 20 C with a mixing time, $T_m = 600$ ns. Spectral reconstruction at decomposition levels of 1 to 4 are shown for the Approximation (A–D) and the Vertical (E–H) components.